Quantifying the role of the eddy transfer coefficient in simulating the response of the Southern Ocean Meridional Overturning Circulation to enhanced westerlies in a coarse-resolution model

Yiwen Li[1,2], Hailong Liu[1,2,3*], Pengfei Lin[1,2], Eric P. Chassignet[4], Zipeng Yu[1,2], Fanghua Wu[5]

[1]State Key Laboratory of Numerical Modeling for Atmospheric Sciences and Geophysical Fluid Dynamics (LASG), Institute of Atmospheric Physics, Chinese Academy of Sciences, Beijing 100029, China

[2]College of Earth and Planetary Sciences, University of Chinese Academy of Sciences, Beijing 100049, China

[3]Center for Ocean Mega-Science, Chinese Academy of Sciences, Qingdao 266071, China

[4]Center for ocean-Atmospheric Prediction Studies, Florida State University, Tallahassee 32306, Florida

[5]National Climate Center, China Meteorological Administration, Beijing 100081, China

* Corresponding author: Hailong Liu (lhl@lasg.iap.ac.cn)

Abstract

The ability of a coarse-resolution ocean model to simulate the response of the Southern Ocean Meridional Overturning Circulation (MOC) to enhanced westerlies is evaluated as a function of the eddy transfer coefficient (κ), which is commonly used to parameterize the bolus velocities induced by unresolved eddies (Gent and McWilliams, 1990). By comparing five different schemes for κ, it is shown that a stratification-dependent and spatiotemporally varying coefficient leads to the largest response of the eddy-induced MOC; however, it accounts for only 65% of the reference eddy-resolving simulation. A comparison between spatially and spatiotemporally varying κ further indicates the more important role of the temporal variation of κ in simulating the response of the eddy compensation. By decomposing the eddy-induced velocity into a new term derived from the introduction of the vertical variation of κ (VV) and an already existing term based on κ (spatial structure, SS), the largest response of the eddy compensation is attributed to the significantly intensified SS term rather than the VV term. The introduction of spatiotemporal κ also makes the response of the density slope, which is a secondary impact of κ, become the key factor to simulate the eddy compensation response precisely, whereas the experiments with constant schemes are determined by κ itself.

1. Introduction

The Southern Ocean crucially connects three basins through its meridional overturning circulation (MOC) and the Antarctic Circumpolar Current (ACC). It is also filled with mesoscale eddies, which can significantly affect the Southern Ocean through altering the volume transport (Gent, 2016), the water mass formation (Waugh, 2014), and the carbon absorption (Swart et al., 2014). The Southern Ocean MOC consists of two cells: the upper cell and the lower cell. The upper cell is driven by both the upwelling of North Atlantic deep waters and the wind-induced northward surface Ekman transport. With global warming and ozone depletion, the Southern Hemisphere westerlies shifted poleward and intensified by ~20%, as shown by satellite data and atmospheric reanalysis (Swart and Fyfe, 2012; Bracegirdle et al., 2013; Farneti et al., 2015; Gent, 2016). The intensified westerlies are thought to enhance the circulations in the Southern Ocean predicted by the wind-driven circulation theory (Speer et al., 2000; Abernathey et al., 2011), but the density slope from the Argo observations (Boning et al., 2008) and the ACC transport from high-resolution simulations (Hallberg and Ganadesikan, 2006; Meredith et al., 2012) do not show a corresponding enhancement. It is usually believed that the input energy from the wind is compensated for by mesoscale eddies in the Southern Ocean, which absorb energy from the westerlies and are also enhanced by the intensified westerlies (Viebahn and Eden, 2010; Hofmann and Maqueda, 2011; Downes and Hogg, 2013; Gent, 2016). The eddy compensation can further affect the Southern Ocean sea surface temperature (SST) by dampening its response to enhanced westerlies (Doddridge et al., 2019). Thus, the Southern Ocean eddy compensation and its response to changes in the westerlies have a crucial role in the state of the Southern Ocean.

To simulate the eddy compensation properly, eddy parameterization is still needed, as most climate models still use non-eddy-resolving ocean models. The eddy-induced transport is commonly parameterized by both the diffusivity (Redi, 1982) and the bolus velocities (Gent and McWilliams, 1990, hereafter referred to as GM), or the skewness flux (Griffies, 1998), with an eddy transfer coefficient (κ). To parameterize the eddy compensation, κ should be variable in both space and time (Gent, 2016). This has been reported from the analysis of multiple non-eddy-resolving simulations with different ocean models and with different GM eddy transfer coefficients, including mixing length scale (Visbeck et al., 1997; Eden and Greatbatch, 2008), the buoyance-dependent scale (Ferreira et al., 2005), and the geometric scale (Marshall et al., 2012). The idealized configuration also indicates that κ should be proportional to the square root of the wind stress to simulate the eddy compensation (Abernathey et al., 2011). Although most studies indicate that one specified character of κ should be included to simulate the eddy compensation properly, it is not clear which feature makes the major contribution. Therefore, it is necessary to quantify the impact of the specified character of κ and its mechanism.

Even though the spatiotemporally varying κ can simulate the eddy compensation in a coarse-resolution model, the magnitudes of the eddy compensation response among previous studies still show inconsistencies. Hofmann and Maqueda (2011) showed a 67% increase in the eddy-induced MOC with doubled westerlies and a length-scale-dependent scheme for κ, whereas Gent and Danabasoglu (2011) showed a 60% eddy compensation with only 50% enhanced westerlies and a buoyancy-dependent scheme by using a coupled model. Furthermore, Downs et al. (2018) showed that the residual upper cell increases by 0.1 to 1.6 Sv per decade among 12 COERII models with different schemes for κ. That spread of the simulated trends of the eddy compensation is due to the different schemes for κ and the different dynamic cores of the models. To evaluate the spread of the simulated eddy compensation in a coarse-resolution model, the eddy-resolving model is usually taken as a reference, as most state-of-the-art eddy-resolving ocean models can resolve the impact of mesoscale eddies on the response of the MOC to enhanced westerlies (Marshall and Radko, 2003; Hallberg and Gnanadesikan 2006; Abernathey et al., 2011; Meredith et al., 2012; Bishop et al., 2016; Gent, 2016; Paulsen et al., 2018). To avoid the effects of the different models' dynamic cores, a comparison between the high- and low-resolution configurations based on one particular model will be helpful to evaluate how much of the effect of eddies in the eddy-resolving model can be parameterized by the coarse-resolution experiments with different schemes for κ. This evaluation will also be useful to understand what features of κ are crucial to parameterize the mesoscale eddies.

This study quantifies the response of the Southern Ocean MOC to increased westerlies in an ocean model with parameterized eddy effects by using different κ. An eddy-resolving configuration is used as the reference to quantify the impact of κ on the simulation of the eddy compensation. Specifically, we look at the effects of two widely used schemes of κ: one depending on the buoyancy frequency from Ferreira et al. (2005) and one depending on time and length scales provided by the eddy growth rate, the Rossby radius of deformation, and the Rhines scale from Eden and Greatbatch (2008). We find that (1) the stratification-dependent κ, especially its temporal variation, strengthens the eddy compensation response to enhanced westerlies in the Southern Ocean, (2) the largest simulated eddy compensation response among the coarse-resolution experiments with different κ accounts for only 65% of that from the reference eddy-resolving experiment, and (3) owing to the introduction of the spatiotemporal variation of κ, the simulation of the eddy compensation response is determined by the response of the density slope rather than κ, which is the dominant factor in experiments with constant κ.

The remainder of the paper is organized as follows. Section 2 describes the ocean model, experiments, and methods of decomposing the eddy-resolving output into the eddy-induced and Eulerian mean transports. In section 3, the response of the circulation to the intensified westerlies in the eddy-resolving model and a coarse-resolution model with different κ are investigated. Section 4 describes how the eddy compensation response in the Southern Ocean is influenced by κ. The last section is the summary and discussion.

2. Experiments and methods

2.1 Eddy-resolving experiment

The ocean model used in this paper was developed at the State Key Laboratory of Numerical Modeling for Atmospheric Sciences and Geophysical Fluid Dynamics (LASG), Institute of Atmospheric Physics (IAP), and named the LASG/IAP Climate system Ocean Model (LICOM). The eddy-resolving experiment uses LICOM version 2.0 (LICOM2.0, Liu et al., 2012), with a 0.1° × 0.1° horizontal grid and 55 vertical levels. In the upper 300 m, 36 levels are used with an average layer thickness of less than 10 m. Biharmonic viscosity and diffusivity schemes are used in the momentum and tracer equations, respectively. The model domain covers 79°S–66°N, excluding the Arctic Ocean. There is a 5° buffer zone at 66°N, where temperature and salinity are restored to the climatological monthly temperature and salinity (Levitus and Boyer, 1994). The experiment, called LICOMH hereafter, was conducted after 12-year spin-up and using the 60-year (1948-2007) daily Coordinated Ocean-Ice Reference

Experiments (CORE, Large and Yeager, 2004) interannually varying forcing. Please refer to Yu et al. (2012) and Liu et al. (2014) for the details of the model description and basic performances.

2.2 Coarse resolution experiments

The coarse resolution experiments use version 3.0 of LICOM (LICOM3, Lin et al., 2020; Li et al., 2020), which is coupled to the Community Ice Code version 4 (CICE4) through the NCAR flux coupler version 7 (CPL7), with approximately 1° horizontal resolution and 30 vertical levels. The vertical resolution is uniform in the top 150 m, with a grid spacing of 10 m, whereas the spacing is uneven below 150 m. The horizontal model grid uses a tripole grid (Murray, 1996) with two poles in the Northern Hemisphere, which are located at 65°N, 30°W and 65°N, 150°E, respectively. The tidal mixing parameterization scheme of St. Laurent et al. (2002) is implemented. The coarse-resolution experiments (hereafter referred to as LICOML) follow the second phase of the Coordinated Ocean-Ice Reference Experiments (COREII) protocol, forced by six-hourly atmospheric data and the bulk formula of Large and Yeager (2009). These experiments are integrated for 124 years, with two 62-year CORE-II cycles, and the second cycle is used for analysis here.

There are five coarse-resolution ocean–sea ice coupled experiments with different schemes for κ (listed in Table 1) to evaluate the influence of κ. The first two coarse-resolution experiments use a constant κ of 500 m^2 s^{-1} and 1000 m^2 s^{-1}, referred to as K500 and K1000, respectively. The next two experiments use an eddy transfer coefficient scheme based on the structure of buoyancy frequency as described in Ferreira et al. 2005 (referred to as FMH hereafter):

$$\kappa = \frac{N^2}{N_{\mathrm{ref}}^2}\kappa_{\mathrm{ref}} \qquad (1)$$

where κ is the eddy transfer coefficient, κ_{ref} is constant and set to 4000 m^2 s^{-1}, N^2 is the buoyancy frequency, and N_{ref}^2 is the reference buoyancy frequency at the bottom of the mixed layer depth. In the two experiments, called FMH3D and FMH4D, the eddy transfer coefficients are spatially varying and spatiotemporally varying, respectively.

Table 1. The configurations of the experiments

Experiment	Resolutions (°)	κ (m^2/s)	Periods	Forcing
LICOMH	0.1	-	1949-2007	CORE II
K500	1	500	1948-2009	CORE II
K1000	1	1000	1948-2009	CORE II
FMH3D	1	$\overline{\kappa_{ref}(N^2/N_{ref}^2)}$	1948-2009	CORE II
FMH4D	1	$\kappa_{ref}(N^2/N_{ref}^2)$	1948-2009	CORE II
EG	1	$\alpha\sigma(x,y,z)L^2(x,y,z)$	1948-2009	CORE II

The fifth coarse-resolution experiment uses the scheme of κ from Eden and Greatbatch (2008), which is computed from time and length scales derived from the eddy growth rate, the Rossby radius of deformation, and the Rhines scale:

$$\kappa = \alpha\sigma(x,y,z)L^2(x,y,z) \tag{2}$$

where σ denotes an inverse eddy timescale that is given by the eddy growth rate; L is an eddy length scale, which is the minimum of the local Rossby radius of deformation and the Rhines scale; and α is a constant parameter of order one following Eden and Greatbatch (2008) and Eden et al. (2009). The experiment is called EG hereafter.

The coefficient for isopycnal mixing (Redi, 1982) is the same for all experiments with a constant value of 500 $m^2\ s^{-1}$ — this has been shown to impact the response of the Southern Ocean MOC to the enhanced westerlies (Abernathey and Ferreira, 2015).

2.3 Decomposition of MOC in LICOMH

The total MOC, also named the residual MOC, consists of the Eulerian and the eddy-induced MOC. Following Poulsen et al. (2018), the eddy-induced MOC in LICOMH is defined by the deviation of the total MOC from the Eulerian MOC calculated based on time-mean velocities. As in previous studies, we perform the decomposition analysis in the isopycnal coordinate system (e.g., Hallberg and Gnanadesikan, 2006; Munday et al., 2013; Bishop et al., 2016; Poulsen et al., 2018).

The residual MOC during one period is given by:

$$\psi(\theta,\rho)_{\mathrm{res}} = \overline{\oint_0^{2\pi} \int_{\rho_{\mathrm{T}}(\phi,\theta,t)}^{\rho(\phi,\theta,t)} v(\phi,\theta,\rho,t)\mathrm{d}\rho R cos(\theta)\mathrm{d}\phi} \tag{3}$$

where v is the meridional velocity, ϕ and θ are the usual spherical coordinates, R is Earth's radius, and ρ is the potential density. ρ_{T} is the potential density of the ocean top, and $\rho(\phi,\theta,t)$ is the potential density surface, which varies in both space and time. $\overline{(\,)}$ denotes the average operator over time. The vertical integration here is from the top to the bottom. The potential density is calculated with a reference pressure of 2000 dbar.

To obtain the Eulerian MOC, the decomposition is applied to the velocity and the density field first, which results in a time-mean field and its deviation (or eddy-induced values). Taking the meridional velocity as an example, we define the decomposition as follows:

$$v(\phi,\theta,\rho,t) = \bar{v}(\phi,\theta,\rho) + v^*(\phi,\theta,\rho,t) \tag{4}$$

where $\bar{v}$ is the time-mean meridional velocity and v^* is the eddy-induced meridional velocity. The stream function derived from the time-mean field represents the Eulerian mean overturning circulation and is given by:

$$\psi(\theta,\rho)_{\mathrm{Euler}} = \oint_0^{2\pi} \int_{\overline{\rho_{\mathrm{T}}}(\phi,\theta)}^{\bar{\rho}(\phi,\theta)} \bar{v}(\phi,\theta,\rho)\mathrm{d}\rho R cos(\theta)\mathrm{d}\phi \tag{5}$$

where $\bar{v}$ is the time-mean velocity, $\bar{\rho}$ is the time-mean potential density, and $\overline{\rho_T}$ is the time-mean potential density of the ocean top.

Finally, the difference between the residual MOC ψ_{res} and the Eulerian MOC ψ_{Euler} is the eddy-induced MOC:

$$\psi^* = \psi_{\mathrm{res}} - \psi_{\mathrm{Euler}} \tag{6}$$

which captures the motion that varies on a temporal timescale shorter than the period of the applied time-averaging operator. As in Poulsen et al. (2018), we use monthly average outputs to calculate the eddy-induced circulation.

3. Results

3.1 Enhanced westerlies

Figure 1a shows the 12-month running mean monthly series of the zonal wind stress averaged in the Southern Ocean (40–60°S and 0–360°E) and its linear trend for LICOML. The wind stress was computed using CORE II forcing and model-predicted SST, which indicates an increasing trend from 1949 to 2007 with a magnitude of about 0.008 N m^{-2} per decade (significant by Mann–Kendall non-parametric test). The trend is consistent with the enhanced westerlies in the Southern Ocean that appeared during recent decades found in previous studies (Swart and Fyfe, 2012; Bracegirdle et al., 2013; Farneti et al., 2015; Gent, 2016). The difference in the zonal wind stress between 1998–2007 and 1960–1969 is presented in Figure 1b. There is a general enhancement of the zonal wind stress in the Southern Ocean with a maximum of 0.1 Pa and about 25.2% increase averaged over 40–60°S and 0–360°E. Furthermore, a slightly poleward shift of the zonal wind stress is also shown, which is confirmed by previous studies (e.g., Goyal et al., 2021). This significant multidecadal intensification of westerlies in the Southern Ocean is believed to be driven partially by ozone depletion and global warming (Thompson and Solomon, 2002; Marshall, 2003; Miller et al., 2016). The linear trend of the zonal wind stress in the Southern Ocean from LICOMH is similar to that from LICOML, but with a slightly smaller magnitude of 0.007 Pa per decade. For the comparison between the two periods, LICOMH shows an increase in strength of 23.6%, which is 1.6% weaker than the 25.2% from LICOML. In general, the enhanced westerlies are well simulated in both LICOML and LICOMH (Fig. S1). In terms of the evaluation of the response of the Southern Ocean MOC, it is reasonable to assume that there are same changes in the westerlies for LICOML and LICOMH.

3.2 Response in the eddy-resolving experiment

The response of the Southern Ocean MOC to the intensified westerlies is estimated by the eddy-resolving experiment (LICOMH), in which mesoscale eddies can be resolved implicitly. The first row of Figure 2 shows the residual, Eulerian, and eddy-induced MOC in the isopycnal coordinate system during 1949–2007 in the Southern Ocean. The positive upper cell and the negative lower cell are presented clearly in the residual MOC (Fig. 2a), and are located from 35°S to 55°S near the surface of 36.45 kg m^{-3} and from 35°S to 75°S near the surface of 36.90 kg m^{-3}, respectively. This structure is in line with the theoretical pattern in the isopycnal coordinate system (Farneti et al., 2015). The eddy-induced MOC shows the opposite direction to the Eulerian MOC, compensating for the Eulerian MOC and leading to a weaker clockwise residual MOC in the upper cell, which is consistent with previous studies (e.g., Hallberg and Ganadesikan, 2006; Meredith et al., 2012; Paulsen et al., 2018).

The MOC during 1960–1969 and 1998–2007 is presented in the second and third rows of Figure 2 to evaluate the response of the MOC to enhanced westerlies. The clockwise residual MOC during 1998–2007 (Fig. 2g) has an average strength of 2.77 Sv from 34.0 to 36.85 kg m^{-3} and from 40°S to 60°S, whereas it is 1.05 Sv during 1960–1969 (Fig. 2d), indicating a 1.72 Sv increase of the clockwise residual MOC from 1960–1969 to 1998–2007. To quantify the response, we define the mean value in the area from 34.0 to 36.85 kg m^{-3} and from 40°S to 60°S as an index to measure the strength of the upper cell, which contains the majority of the clockwise MOC during the whole period. There is a 3.83 Sv increase of the strength of the residual MOC from 1960–1969 to 1998–2007 (Fig. 2j and Table. 2), which is an increase of 69% compared with 1960–1969. For the Eulerian MOC in LICOMH, its enhancement is larger than that of the residual MOC, with a strength of 5.77 Sv (Fig. 2k and Table. 2), increasing by 258% compared with 1960–1969. The ratio of 258% is not in line with the ratio of the enhanced westerlies, which may be caused by the changing density slope. In addition, the definition of the MOC strength also affects the magnitude of the ratio. Hence, there are two types of eddy compensation. One considers only the spatial compensation in terms of the MOC, and the other considers that the response of the eddy compensation also shows an intensification, which compensates for the enhancement of the Eulerian MOC.

The difference between the response of the residual MOC and the response of the Eulerian MOC is due to the compensation of the eddy-induced MOC, as Figure 2 shows that the direction of the eddy-induced MOC (Fig. 2c, 2f, and 2i) is opposite to that of the Eulerian MOC (Fig. 2b, 2e, and 2h) in the region of the upper cell. Furthermore, the eddy-induced MOC exhibits enhancement with increasing time between 40°S and 60°S (Fig. 2l), which is −5.89 Sv during 1960–1969 and −6.80 Sv during 1998–2007. The strength of the intensified eddy-induced MOC (referred to as the eddy compensation response) is 0.91 Sv, which makes up to 15.4% of the eddy-induced MOC during 1960–1969. This ratio is smaller than that of the intensified westerlies (23.6%), which may be caused by the varying potential vorticity across the Southern Ocean (Meredith et al., 2012). Therefore, the eddy compensation in the upper cell from LICOMH has an increase of 15.4% from 1960–1969 to 1998–2007.

3.3 Responses in the coarse-resolution experiments

To investigate the performance of the parameterized eddy in the coarse-resolution experiments, we examine five coarse-resolution ocean model experiments with different κ, that is schemes K500, K1000, FMH3D, FMH4D, and EG (Fig. 3d, 3h, 3l, 3p, and 3t). As shown in Figure 3, the climatological mean eddy-induced MOC (the third column) of all five experiments shows anticlockwise circulations during 1948–2009, which is opposite to the Eulerian MOC (the second column). In terms of the κ value, it is expected that a change in value from 500 $m^2\ s^{-1}$ to 1000 $m^2\ s^{-1}$ leads to stronger eddy-induced MOC (Fig. 3c and 3g) and Eulerian MOC (Fig. 3b and 3f). For the eddy transfer coefficients with spatial and temporal variation in the other three experiments (Fig. 3i, 3p, and 3t), the patterns of the residual MOC only change slightly. The slight change in the residual MOC is the result of the compensation between the Eulerian MOC and the eddy-induced MOC, which are sensitive to the κ scheme. Although the climatological residual MOC barely shows sensitivity to the κ scheme, the dependence of the eddy-induced MOC and the Eulerian MOC on the κ scheme may have huge impacts in terms of the climate response.

Figure 4 shows the responses of the residual, Eulerian, and eddy-induced MOC between 1960–1969 and 1998–2007, in which there is an approximately 25.2% enhancement of westerlies in the Southern Ocean. From the first column of Figure 4, it can be seen that there are obvious differences among the responses of the residual MOC in the five experiments with different κ schemes. Furthermore, the changes in the residual MOC in all five experiments (first column in Fig. 4) are smaller than that of the Eulerian MOC (second column in Fig. 4), which is caused by the compensation of the enhanced anticlockwise eddy-induced MOC (third column in Fig. 4). Thus, the eddy compensation can be reflected by the parameterized eddy transport regardless of the κ scheme. However, compared with the other four experiments, FMH4D has the most extensive enhancement and region of the anticlockwise eddy-induced MOC (third column in Fig. 4), which leads to a smaller difference in the residual MOC among the five experiments. The Eulerian MOC also shows sensitivity to κ despite the same change in wind stress, which may be caused by the secondary effects of κ, such as the mixing and the meridional density gradient. The choice of κ scheme shows the crucial role of κ in simulating the response of the MOC.

To quantify the difference among the five experiments, we also use the defined index to measure the strength of the upper cell, which is the average value of the MOC between 34.0 and 36.85 kg m^{-3} and from 40°S to 60°S. The changes in the residual, Eulerian, and eddy-induced MOC between 1960–1969 and 1998–2007 are listed in Table 2. The enhanced eddy compensation for LICOMH is 0.91 Sv, which is about 15.4% of the eddy-induced MOC during 1960–1969. For the coarse-resolution experiments, the FMH4D and EG experiments have a relatively larger eddy compensation of 0.59 Sv and 0.42 Sv, respectively, and relative changes of about 14.5% and 15.3%, which are closer to LICOMH. For the K500, K1000, and FMH3D experiments, the enhanced eddy-induced MOC is smaller, which is 0.26 Sv, 0.38 Sv, and 0.40 Sv, respectively, with relative values of about 10%. This result indicates that the spatiotemporal variance of κ is crucial to the eddy compensation regardless of the κ scheme. In addition, the contrast between FMH3D and FMH4D indicates that the spatially varying κ is not sufficient to simulate the full compensation effect. Besides, the comparison between K500 and K1000 suggests that a larger value of κ leads to stronger eddy compensation.

Although the temporal eddy compensation is simulated in all five experiments, the absolute values of the eddy-induced response of the MOC are all smaller than that of LICOMH. FMH4D has the largest eddy compensation of −0.59 Sv, which accounts for 65% of LICOMH, whereas K500 only makes up 29% of LICOMH. Therefore, the parameterized eddy can simulate only partial eddy compensation from the eddy-resolving model. There is still at least 35% eddy compensation that cannot be simulated by the coarse-resolution experiments.

Table 2 The differences in the strength for the residual, Eulerian, and eddy-induced MOC between 1960–1969 and 1998–2007 for the high-resolution and five coarse-resolution experiments. The ratio of the eddy-induced response of the MOC to the eddy-induced MOC during 1960–1969 is also listed.

Experiments	Residual	Eulerian	Eddy	Ratio
LICOMH	3.83	5.77	-0.91	15.4%
K500	2.01	2.26	-0.26	10.3%
K1000	2.31	2.69	-0.38	9.4%
FMH3D	2.31	2.71	-0.40	9.0%
FMH4D	2.39	2.98	-0.59	14.3%
EG	3.39	3.81	-0.42	15.3%

Note: The strength is the mean value from 34.0 to 36.85 kg m^{-3} and from 40°S to 60°S (Unit: Sv).

On the basis of the comparison above, we found that the eddy compensation has a crucial role in the response of the MOC to the surface wind. Only 65% of the eddy compensation from the reference eddy-resolving experiment can be simulated by the parameterized eddy in the coarse-resolution experiments. The spatiotemporal variation of the buoyancy-dependent κ, especially the temporal variation of κ, is shown to be the more crucial factor in simulating the eddy compensation in the coarse-resolution models. However, how the spatiotemporal variation of the eddy transfer coefficient affects the eddy compensation and why the temporal variation is more important still needs further analysis.

3.4 Influence on the eddy compensation

As shown above, we find that the eddy compensation from the FMH4D and EG experiments is closer to the high-resolution result, whereas the other experiments show weaker eddy compensation. In this section, we further analyze why the eddy transfer coefficients from the FMH4D and EG experiments lead to stronger eddy-induced MOC enhancement.

3.4.1 The attribution of the eddy-induced MOC

The eddy-induced velocity in LICOML is parameterized following Gent and McWilliams (1990).

$$u^* = (\kappa \frac{\rho_x}{\rho_z})_z = (\kappa Slope\_x)_z \tag{7}$$

$$v^* = (\kappa \frac{\rho_y}{\rho_z})_z = (\kappa Slope\_y)_z \tag{8}$$

where u^* and v^* are the zonal and meridional eddy-induced velocity, respectively; κ is the eddy transfer coefficient; and ρ_x, ρ_y, and ρ_z are the partial differential of density in the zonal, meridional, and vertical directions, respectively. Therefore, ρ_x/ρ_z and ρ_y/ρ_z represent the zonal and meridional density slope, represented as $Slope\_x$ and $Slope\_y$.

If κ has vertical variation, the velocity can be decomposed into two terms. The meridional bolus velocity can be presented as:

$$v^* = (\kappa Slope\_y)_z = \kappa(Slope\_y)_z + Slope\_y\kappa_z \tag{9}$$

where the two terms on the right-hand side represent the impact of κ spatial structure (called SS hereafter) and the impact of the vertical variation of κ (called VV hereafter).

The VV term is the newly introduced term owing to the vertical variation of κ, which will vanish in the constant scheme of κ. The terms for the five schemes used in this study are listed in Table 3.

Table 3 The components of the SS and VV terms among the five experiments, and the components of their response.

	SS	VV	ΔSS	ΔVV
K500	$\kappa(Slope\_y)_z$	-	$(Slope\_y)'_z\kappa$	-
K1000	$\kappa(Slope\_y)_z$	-	$(Slope\_y)'_z\kappa$	-
FMH3D	$\kappa(Slope\_y)_z$	$\kappa_z Slope\_y$	$(Slope\_y)'_z\kappa$	$(Slope\_y)'\kappa_z$
FMH4D	$\kappa(Slope\_y)_z$	$\kappa_z Slope\_y$	$(Slope\_y)'_z\kappa$ $+ (Slope\_y)_z\kappa'$ $+ (Slope\_y)'_z\kappa'$	$(Slope\_y)'\kappa_z$ $+ (Slope\_y)\kappa'_z$ $+ (Slope\_y)'\kappa'_z$
EG	$\kappa(Slope\_y)_z$	$\kappa_z Slope\_y$	$(Slope\_y)'_z\kappa$ $+ (Slope\_y)_z\kappa'$ $+ (Slope\_y)'_z\kappa'$	$(Slope\_y)'\kappa_z$ $+ (Slope\_y)\kappa'_z$ $+ (Slope\_y)'\kappa'_z$

Figure 5 shows the eddy-induced MOC due to the SS term among the five experiments during 1960–1969 and the changes between 1960–1969 and 1998–2007. The calculation is same as equation (5) but based on the SS-induced velocity. The SS-induced MOC from the experiments with a constant scheme (K500 and K1000) is the whole eddy-induced MOC, which is a closed circulation (Fig. 5a and 5b). However, for the experiments with spatially varying κ, the values of the SS-induced MOC and their changes are all negative, which contributes to the eddy compensation. On the basis of the comparison among the five experiments in Figure 5, it is clear that the spatially varying κ leads to a stronger SS term than in the constant schemes. In addition, the temporal variation of κ leads to a stronger response of the eddy compensation compared with the spatially varying κ. The MOC strength for the two constant scheme experiments is around 10 Sv (Fig. 5a and 5b), whereas it is larger than 20 Sv for the FMH3D, FMH4D, and EG experiments (Fig. 5c–5e). Compared with the FMH3D scheme, the FMH4D and EG schemes have larger responses, which are larger than 4 Sv between 50°S and 55°S (Fig. 5i and 5j).

Furthermore, the SS-induced MOC for the five schemes also has a different spatial structure. For the constant scheme, the centers of the MOC are located around 55°S and the surface of 36.89 kg m^{-3} with a maximum magnitude of 10 Sv for K500 and 18 Sv for K1000 (Fig. 5a and 5b), whereas the larger than 18 Sv center of the MOC can be found around 40°–60°S and 36.43–36.89 kg m^{-3} for the FMH experiment (Fig. 5c and 5d) and south of 40°S and 36.05–36.89 kg m^{-3} for the EG experiment. In general, their responses occur between 50°S and 55°S (Fig. 5f and 5g), which are also the latitudes of the large wind-stress changes. These differences in the structure of the SS-induced response of the MOC are reflected in the response of the eddy-induced MOC (Fig. 4c, 4g, 4k, 4o, and 4s).

Figure 6 shows the VV-induced MOC during 1960–1969 for experiments with spatially varying schemes and their responses to enhanced westerlies. If we compare the VV term with the SS term (Fig. 5), we find that the VV term and its response is always positive or a clockwise MOC, which compensates for the SS term and leads to a closed circulation. As the VV-induced MOC is opposite to the SS-induced MOC and the eddy-induced MOC, it is the SS term that dominates the eddy-induced MOC. The changes in the VV-induced MOC are all about 3 Sv, which is less than the changes in the SS-induced MOCS, which is about 4 Sv. Therefore, the total responses of the eddy-induced MOC are all approximately 1 Sv or less. The contrast between the SS- and the VV-induced MOC indicates that the eddy compensations for the FMH4D and EG experiments come from the enhanced SS-induced MOC, rather than the introduced VV-induced MOC derived from the vertical variation of κ.

3.4.2 The attribution of the response

The decomposition of the eddy-induced MOC has shown that the SS-induced MOC is the leading factor for the eddy compensation. Furthermore, to investigate the attribution of the SS-induced MOC, Figure 7 shows the components of the SS-induced MOC, which is the SS-induced velocity (V_{ss}) and the thickness of the density layers (hh). The hh among the five experiments is similar, whereas V_{ss} shows a significant difference, which implies that the difference in the SS-induced MOC among the different experiments comes from V_{ss}. Therefore, it is reasonable to evaluate the attribution of the response of the SS-induced MOC through the SS-induced velocity.

On the basis of the decomposition of the eddy-induced velocity, the response of the SS term can also be decomposed as follows:

$$\begin{aligned}\Delta V'_{\mathrm{SS}} &= V_{\mathrm{SS}}(1998\text{-}2007) - V_{\mathrm{SS}}(1960\text{-}1969) \\ &= (\kappa + \kappa')\,[(Slope\_y)_z + (Slope\_y)'_z] - \kappa(Slope\_y)_z \\ &= (Slope\_y)'_z\kappa + (Slope\_y)_z\kappa' + (Slope\_y)'_z\kappa' \qquad (10)\end{aligned}$$

where $\Delta V'_{\mathrm{SS}}$ represents the difference between the 1998–2007 average and the 1960–1969 average SS-eddy-induced velocity. κ is the eddy transfer coefficient during 1960–1969 and κ' is the difference in κ between 1998–2007 and 1960–1969. $(Slope\_y)_z$ is the vertical partial derivative of the meridional density slope during 1960–1969 and $(Slope\_y)'_z$ is the difference of $(Slope\_y)_z$ between 1998–2007 and 1960–1969. The components of the decomposition from all five experiments are listed in Table 3. Even though the spatial and temporal variation of κ show a vital role in the SS-induced MOC, it is not clear whether the better simulations of the response of the eddy-induced MOC for the FMH4D and EG experiments come from κ itself or the density slope, which are two significant components of the eddy-induced velocity.

Figure 8 shows the responses of the SS-induced velocity and its components from the FMH4D and EG experiments. When comparing the response of SS-induced velocity ($\Delta V'_{\mathrm{SS}}$) and its three components, the value and pattern of $(Slope\_y)'_z\kappa$ is almost the same as $\Delta V'_{\mathrm{SS}}$ in both experiments. The spatial correlations between $(Slope\_y)'_z\kappa$ and $\Delta V'_{\mathrm{SS}}$ in FMH4D and EG are 0.98 and 0.96, respectively, and the ratio of $(Slope\_y)'_z\kappa$ to $\Delta V'_{\mathrm{SS}}$ averaged over the whole region can reach 0.83 and 1.31, respectively. The other two components $(Slope\_y)_z\kappa'$ and $(Slope\_y)'\kappa'_z$ show much smaller spatial correlations and ratios in both experiments. Thus, the dominant component of $\Delta V_{SS}'$ is $(Slope\_y)_z'\kappa$, which represent the response of the density slope. This also means the SS-induced response in the experiments with spatiotemporal κ mainly comes from the response of the density slope rather than the response of the eddy transfer coefficient.

In summary, the SS-induced circulation from the FMH4D and EG experiments, leading to stronger eddy compensation, can be traced back to the response of the density slope from the two experiments.

3.5 The influence on the density slope

As analyzed in section 3.4.2, the response of the density slope is the dominant factor leading to the SS-induced response, strengthening the eddy compensation in the FMH4D and EG experiments. This implies that the better simulations of the response of the Southern Ocean MOC to the enhanced westerlies in FMH4D and EG do not come from the spatiotemporally varying κ directly but from the vertical variation of the density slope, which is the secondary impact of κ.

Figure 9 shows the meridional density slope, the vertical variation of the meridional density slope during 1960–1969, and their responses from 1960–1969 to 1998–2007 among the five experiments. For the impact of the value of κ, a larger value leads to a smaller meridional density slope (comparing K1000 with K500, Fig. 9a and Fig. 9b). Furthermore, the value of κ has the same impact on the response of the density slope (Fig. 9f and 9g), the vertical variation of the density slope (Fig. 9k and 9l), and its response (Fig. 9p and 9q).

In experiments with constant κ, the response of the eddy-induced MOC has only two components, which are κ and the vertical variation of the density slope (Table. 3). With a smaller vertical variation of the density slope, K1000 still has stronger eddy compensation than K500 (Table 2), which is caused by its larger value of κ. Thus, the dominant factor in simulating the eddy compensation response among constant schemes is the value of κ itself, rather than its secondary effect.

Comparing FMH4D with FMH3D, the additional temporal variation of κ leads to a stronger enhancement of the density slope and its vertical variation. In addition, FMH4D has a stronger eddy compensation response than FMH3D (Table 2), which confirms that the temporal variation of the density slope's vertical variation is the major factor for the eddy compensation response from experiments with spatially varying κ. The EG experiment shows a larger response of the density slope's vertical variation than FMH4D, even though the eddy compensation from EG is weaker than that from FMH4D (Table 2). The reason for this is that the larger response of the density slope's vertical variation not only causes the stronger response of the SS-induced velocity in EG but also leads to a stronger VV-induced velocity, which counteracts the effect of the SS term. Thus, in experiments with spatially varying κ, the simulation of the density slope's vertical variation is the key to simulating the eddy compensation precisely.

4. Summary and Discussion

In this study, we quantify the influence of five eddy transfer coefficients on the response of the Southern Ocean MOC to intensified westerlies in a non-eddy-resolving ocean model driven by CORE-II forcing. We show that the experiment with a spatially and temporally varying coefficient based on the buoyancy frequency has the closest Southern Ocean MOC response to the eddy-resolving numerical simulation used as a reference. However, the parameterized eddy effect can only simulate 65% of the eddy compensation response in the reference eddy-resolving model.

The ratios between the response of the eddy-induced MOC and its strength during 1960–1969 from the five experiments are calculated to quantify the impact of the eddy transfer coefficient's spatial and temporal variations. We find that the spatial and temporal variability in buoyancy-dependent κ leads to a two-times-stronger eddy compensation response than constant κ (2.3 times more than K500 and 1.6 times more than K1000). Despite the importance of the spatial and temporal variations of κ for simulating the eddy compensation response, the temporal variance of κ is more important than its spatial variance from comparing the eddy compensation response from FMH3D with that from FMH4D. In addition, the contrast between FMH4D and EG implies a more dominant role of the buoyancy feature of κ. This is probably because the buoyancy structure can reflect the feature of the density slope, as the density slope's vertical variation is the key factor to simulate the eddy compensation in experiments with spatiotemporal κ.

A full decomposition of the response of the eddy-induced MOC from the experiments with spatiotemporal κ indicates that the enhanced eddy compensation response is primarily attributed to the response of the density slope, which is a secondary factor induced by κ. However, for constant schemes, the coefficient itself is the dominant factor to simulate the eddy compensation response precisely. Thus, the introduction of the spatiotemporal variation of κ changes the mechanism of its impact on the Southern Ocean MOC. Future work to improve the simulation of the eddy compensation can focus on the improvement of the simulation of the density slope rather than the eddy transfer coefficient.

The present results show that stratification-based and scale-based schemes that allow for spatial and temporal variability improve the simulation of the Southern Ocean circulation's response to climate change by affecting the simulation of the density slope, which represents the baroclinic instability and the energy source of mesoscale eddies. However, the strength of the residual MOC and the Eulerian MOC shows that there is still a huge difference between LICOMH and the five coarse-resolution experiments. This may be caused by the different buoyancy flux between LICOMH and LICOML, as the sea ice is coupled in LICOML. Furthermore, even though the Southern Ocean circulation's response in the FMH4D experiment is close to that of the eddy-resolving ocean model, it cannot be guaranteed that the eddy-resolving model is the truth as different eddy-resolving models show different results (Bishop et al., 2016; Poulsen et al., 2018). Therefore, it will be meaningful to evaluate the eddy compensation in different eddy-resolving models, to gain a more realistic reference for the coarse-resolution climate ocean model.

Acknowledgments

Drs. Li, Liu, Lin, and Yu are supported by National Key R&D Program for Developing Basic Sciences (2018YFA0605703, 2016YFC1401401, 2016YFC1401601) and the National Natural Science Foundation of China (Grants 41931183 and 41776030). Dr. Chassignet is supported by the CAS President's International Fellowship Initiative (PIFI) and NOAA Climate Program Office MAPP Program (Award NA15OAR4310088). The data used in this paper can be downloaded from https://osf.io/nr4yf/.

References

Abernathey, R. P., & Ferreira, D. (2015). Southern Ocean isopycnal mixing and ventilation changes driven by winds, Geophys. Res. Lett., 42, 10,357–10,365, doi:10.1002/2015GL066238.

Abernathey, R. P., & Marshall, J. (2013). Global surface eddy diffusivities derived from satellite altimetry. Journal of Geophysical Research: Oceans, 118(2), 901-916. https://doi.org/10.1002/jgrc.20066

Abernathey, R.P., Marshall, J., & Ferreira, D. (2011). The dependence of Southern Ocean meridional overturning on wind stress. Journal of Physical Oceanography, 41(12), 2261-2278.

Bishop, S. P., Gent, P. R., Bryan, F. O., Thompson, A. F., Long, M. C., & Abernathey, R. (2016). Southern Ocean overturning compensation in an eddy-resolving climate simulation. Journal of Physical Oceanography, 46(5), 1575-1592. https://doi.org/10.1175/JPO-D-15-0177.1

Böning, C. W., Dispert, A., Visbeck, M., Rintoul, S. R., & Schwarzkopf, F. U. (2008). The response of the Antarctic Circumpolar Current to recent climate change. Nature Geoscience, 1(12), 864-869.

Bracegirdle, T. J., Shuckburgh, E., Sallee, J. B., Wang, Z., Meijers, A. J., Bruneau, N., ... & Wilcox, L. J. (2013). Assessment of surface winds over the Atlantic, Indian, and Pacific Ocean sectors of the Southern Ocean in CMIP5 models: Historical bias, forcing response, and state dependence. Journal of Geophysical Research: Atmospheres, 118(2), 547-562. https://doi.org/10.1002/jgrd.50153

Danabasoglu, G., & Marshall, J. (2007). Effects of vertical variations of thickness diffusivity in an ocean general circulation model. Ocean Modelling, 18(2), 122-141.

Doddridge, E. W., Marshall, J., Song, H., Campin, J.-M., Kelley, M., & Nazarenko, L.

S. (2019). Eddy compensation dampens Southern Ocean sea surface temperature response to westerly wind trends. Geophysical Research Letters, 46, 4365– 4377

Downes, S. M., & Hogg, A. M. (2013). Southern Ocean circulation and eddy compensation in CMIP5 models. Journal of Climate, 26(18), 7198-7220.

Downes, S. M., Spence, P., & Hogg, A. M. (2018). Understanding variability of the Southern Ocean overturning circulation in CORE-II models. Ocean Modelling, 123, 98-109. https://doi.org/10.1016/j.ocemod.2018.01.005

Eden, C., Jochum, M., & Danabasoglu, G. (2009). Effects of different closures for thickness diffusivity. Ocean Modelling, 26(1-2), 47-59. https://doi.org/10.1016/j.ocemod.2008.08.004

Eden, C., & Greatbatch, R. J. (2008). Towards a mesoscale eddy closure. Ocean Modelling, 20(3), 223-239. https://doi.org/10.1016/j.ocemod.2007.09.002

Eden, C., Jochum, M., & Danabasoglu, G. (2009). Effects of different closures for thickness diffusivity. Ocean Modelling, 26(1-2), 47-59. https://doi.org/10.1016/j.ocemod.2008.08.004

Farneti, R., & Gent, P. R. (2011). The effects of the eddy-induced advection coefficient in a coarse-resolution coupled climate model. Ocean Modelling, 39(1-2), 135-145. https://doi.org/10.1016/j.ocemod.2011.02.005

Farneti, R., Downes, S. M., Griffies, S. M., Marsland, S. J., Behrens, E., Bentsen, M., ... & Canuto, V. M. (2015). An assessment of Antarctic Circumpolar Current and Southern Ocean meridional overturning circulation during 1958–2007 in a suite of interannual CORE-II simulations. Ocean Modelling, 93, 84-120. https://doi.org/10.1016/j.ocemod.2015.07.009

Ferreira, D., Marshall, J., & Heimbach, P. (2005). Estimating eddy stresses by fitting dynamics to observations using a residual-mean ocean circulation model and its adjoint. Journal of Physical Oceanography, 35(10), 1891-1910. https://doi.org/10.1175/JPO2785.1

Gent, P. R. (2016). Effects of Southern Hemisphere wind changes on the meridional overturning circulation in ocean models. Annual review of marine science, 8, 79-94. https://doi.org/10.1146/annurev-marine-122414-033929

Gent, P. R., & Danabasoglu, G. (2011). Response to increasing Southern Hemisphere winds in CCSM4. Journal of climate, 24(19), 4992-4998. https://doi.org/10.1175/JCLI-D-10-05011.1

Gent, P. R., & Mcwilliams, J. C. (1990). Isopycnal mixing in ocean circulation models. Journal of Physical Oceanography, 20(1), 150-155. https://doi.org/10.1175/1520-0485(1990)020<0150:IMIOCM>2.0.CO;2

Goyal, R., Gupta, A. S., Jucker, M., & England, M. H. (2021). Historical and projected changes in the Southern Hemisphere surface westerlies. Geophysical Research Letters, 48, e2020GL090849. https://doi.org/10.1029/2020GL090849

Hallberg, R., & Gnanadesikan, A. (2006). The role of eddies in determining the structure and response of the wind-driven Southern Hemisphere overturning: Results from the Modeling Eddies in the Southern Ocean (MESO) project. Journal of Physical Oceanography, 36(12), 2232-2252.

https://doi.org/10.1175/JPO2980.1

Hofmann, M., & Morales Maqueda, M. A. (2011). The response of Southern Ocean eddies to increased midlatitude westerlies: A non-eddy resolving model study. Geophysical Research Letters, 38(3). https://doi.org/10.1029/2002GL015919

Kalnay, E., Kanamitsu, M., Kistler, R., Collins, W., Deaven, D., Gandin, L., ... & Zhu, Y. (1996). The NCEP/NCAR 40-year reanalysis project. Bulletin of the American meteorological Society, 77(3), 437-472.

Large, W. G., & Yeager, S. G. (2004). Diurnal to decadal global forcing for ocean and sea-ice models: the data sets and flux climatologies. NCAR Technical Note. National Center for Atmospheric Research, 11, 324-336. https://doi.org/10.5065/D6KK98Q6

Large, W. G., & Yeager, S. G. (2009). The global climatology of an interannually varying air–sea flux data set. Climate dynamics, 33(2-3), 341-364. https://doi.org/10.1007/s00382-008-0441-3

Levitus, S., and T. P. Boyer (1994). World Ocean Atlas 1994, vol. 4, Temperature, NOAA Atlas NESDIS 4, 129 pp., Natl. Oceanic and Atmos. Admin., Silver Spring, Md.

Laurent, S., L. C., Simmons, H., & Jayne, S. (2002). Estimating tidally driven mixing in the deep ocean. Geophys. Res. Lett., 29, 21-1–21-4, doi: 10.1029/2002GL015633.

Li, Y., Liu, H., Ding, M., Lin, P., Yu, Z., Yu, Y., ... & Chen, K. (2020). Eddy-resolving Simulation of CAS-LICOM3 for Phase 2 of the Ocean Model Intercomparison Project. Advances in Atmospheric Sciences, 37(10), 1067-1080.

Lin, P., Yu, Z., Liu, H., Yu, Y., Li, Y., Jiang, J., Xue, W., Chen, K., Yang, Q., Zhao, B. and Wei, J. (2020). LICOM Model Datasets for the CMIP6 Ocean Model Intercomparison Project. Advances in Atmospheric Sciences, 37(3), pp.239-249.

Liu, H., Lin, P., Yu, Y., & Zhang, X. (2012). The baseline evaluation of LASG/IAP climate system ocean model (LICOM) version 2. Acta Meteorologica Sinica, 26(3), 318-329. https://doi.org/10.1007/s13351-012-0305-y

Liu, H., Yu, Y., Lin, P., & Wang, F. (2014). High-resolution LICOM. In Flexible Global Ocean-Atmosphere-Land System Model (pp. 321-331). Springer, Berlin, Heidelberg. https://doi.org/10.1007/978-3-642-41801-3_38

Marshall, G. J. (2003). Trends in the Southern Annular Mode from observations and reanalyses. Journal of Climate, 16(24), 4134-4143. https://doi.org/10.1175/1520-0442(2003)016<4134:TITSAM>2.0.CO;2

Marshall, J., & Radko, T. (2003). Residual-mean solutions for the Antarctic Circumpolar Current and its associated overturning circulation. Journal of Physical Oceanography, 33(11), 2341-2354. https://doi.org/10.1175/1520-0485(2003)033<2341:RSFTAC>2.0.CO;2

Marshall D P, Maddison J R, Berloff P S. (2012). A framework for parameterizing eddy potential vorticity fluxes[J]. Journal of Physical Oceanography, 42(4): 539-557.

Meredith, M. P., & Hogg, A. M. (2006). Circumpolar response of Southern Ocean eddy activity to a change in the Southern Annular Mode. Geophysical Research

Letters, 33(16). https://doi.org/10.1029/2006GL026499

Meredith, M. P., Naveira Garabato, A. C., Hogg, A. M., & Farneti, R. (2012). Sensitivity of the overturning circulation in the Southern Ocean to decadal changes in wind forcing. Journal of Climate, 25(1), 99-110. https://doi.org/10.1175/2011JCLI4204.1

Miller, R. L., Schmidt, G. A., & Shindell, D. T. (2006). Forced annular variations in the 20th century intergovernmental panel on climate change fourth assessment report models. Journal of Geophysical Research: Atmospheres, 111(D18). doi:10.1029/2005JD006323

Munday, D. R., Johnson, H. L., & Marshall, D. P. (2013). Eddy saturation of equilibrated circumpolar currents. Journal of Physical Oceanography, 43(3), 507-532. https://doi.org/10.1175/JPO-D-12-095.1

Murray, R. J. (1996). Explicit generation of orthogonal grids for ocean models. Journal of Computational Physics, 126(2), 251-273. https://doi.org/10.1006/jcph.1996.0136

Poulsen, M. B., Jochum, M., & Nuterman, R. (2018). Parameterized and resolved Southern Ocean eddy compensation. Ocean Modelling, 124, 1-15. https://doi.org/10.1016/j.ocemod.2018.01.008

Redi, M. H. (1982). Oceanic Isopycnal Mixing by Coordinate Rotation, Journal of Physical Oceanography, 12(10), 1154-1158.

Smith, R. D., & Gent, P. R. (2004). Anisotropic Gent–McWilliams parameterization for ocean models. Journal of Physical Oceanography, 34(11), 2541-2564. https://doi.org/10.1175/JPO2613.1

Speer, K., Rintoul, S. R., & Sloyan, B. (2000). The diabatic Deacon cell. Journal of physical oceanography, 30(12), 3212-3222. https://doi.org/10.1175/1520-0485(2000)030<3212:TDDC>2.0.CO;2

St. Laurent, L. C., Simmons, H. L., & Jayne, S. R. (2002). Estimating tidally driven mixing in the deep ocean. Geophysical Research Letters, 29(23), 21-1. https://doi.org/10.1029/2002GL015633

Swart, N. C., & Fyfe, J. C. (2012). Observed and simulated changes in the Southern Hemisphere surface westerly wind-stress. Geophysical Research Letters, 39(16). https://doi.org/10.1029/2012GL052810

Swart, N. C., Fyfe, J. C., Saenko, O. A., & Eby, M. (2014). Wind-driven changes in the ocean carbon sink. Biogeosciences, 11(21), 6107-6117. DOI: 10.5194/bg-11-6107-2014

Thompson, D. W., & Solomon, S. (2002). Interpretation of recent Southern Hemisphere climate change. Science, 296(5569), 895-899. DOI: 10.1126/science.1069270

Viebahn, J., & Eden, C. (2010). Towards the impact of eddies on the response of the Southern Ocean to climate change. Ocean Modelling, 34(3-4), 150-165.

Visbeck M, Marshall J, Haine T, Spall M. (1997) Specification of Eddy Transfer Coefficients in Coarse-Resolution Ocean Circulation Models. Journal of Physical Oceanography, 27(3):381-402.

Waugh, D. W. (2014). Changes in the ventilation of the southern oceans. Philosophical Transactions of the Royal Society A: Mathematical, Physical and Engineering

Sciences, 372(2019), 20130269.
Yu, Y., Liu, H., & Lin, P. (2012). A quasi-global 1/10 eddy-resolving ocean general circulation model and its preliminary results. Chinese Science Bulletin, 57(30), 3908-3916. https://doi.org/10.1007/s11434-012-5234-8

Figure Captions

Figure 1 (a) The black line is the 12-month running mean zonal wind stress averaged in the Southern Ocean (40°S–60°S and 0–360°E) from LICOML. The thick black line is the linear trend of the monthly series. (b) The differences of the zonal wind stress from LICOML between periods of 1998–2007 and 1960–1969, and the zonally averaged values. The red solid and blue dashed lines are for 1960–1969 and 1998–2007, respectively.

Figure 2 The first column is the MOC of residual currents for the periods of (a) 1949–2007, (d) 1960–1969, (g) 1998–2007, and (j) the difference between 1998–2007 and 1960–1969 for LICOMH in the isopycnal coordinate. The black curves represent the zonally averaged isobaths (200, 400, 1000, 1500, 2000, and 3000 m) in the isopycnal coordinate. The second and third columns are the same as the first column, but for the Eulerian MOC and the eddy-induced MOC, respectively. (Unit: Sv)

Figure 3 The top panel is the (a) the residual MOC, (b) the Eulerian MOC, (c) the eddy-induced MOC and (d) the eddy transfer coefficient (κ) for the K500 experiment during 1948–2009. The second to the bottom rows are for the K1000, FMH3D, FMH4D, and EG experiments, respectively. The gray lines represent the zonally averaged isobaths (200, 400, 1000, 1500, 2000, and 3000 m) in the isopycnal coordinate system. (Unit: Sv)

Figure 4 The first row is the difference of the (a) the residual MOC, (b) the Eulerian MOC, (c) the eddy-induced MOC, and (d) the eddy transfer coefficient ($\Delta\kappa$) between 1960–1969 and 1998–2007 for the K500 experiment. The gray lines represent the zonally averaged isobaths (200, 400, 1000, 1500, 2000, and 3000 m) in the isopycnal coordinate system. The second to the bottom rows are for K1000, FMH3D, FMH4D, and EG experiments, respectively. (Unit: Sv)

Figure 5 The left column is the SS-induced MOC during 1960–1969 for (a) K500, (b) K1000, (c) FMH3D, (d) FMH4D, and (e) EG. The right column is the difference in the SS-induced MOC between 1960–1969 and 1998–2007 for the five experiments. The gray lines in the left column are the zonally averaged isobaths (200, 400, 1000, 1500, 2000, and 3000 m) in the isopycnal coordinate system. (Unit: Sv)

Figure 6. The left column is the VV-induced MOC during 1960–1969 for (a) FMH3D, (b) FMH4D, and (c) EG. The right column is the difference in the VV-induced MOC between 1960–1969 and 1998–2007 for the three experiments. The gray lines in the left column are the zonally averaged isobaths (200, 400, 1000, 1500, 2000, and 3000 m) in the isopycnal coordinate system. (Unit: Sv)

Figure 7. The left panels from top to bottom are the zonally integrated SS-induced velocities (m s^{-1}) during 1960–1969 for (a) K500, (b) K1000, (c) FMH3D, (d) FMH4D, and (e) EG. The right panels are the zonally integrated thicknesses of the density layers (m) during 1960–1969 for the five experiments.

Figure 8. The left column is (a) the difference of the SS term induced velocity ($\Delta V'_{SS}$) between 1960–1969 and 1998–2007 for the FMH4D experiment and its three components (b) $(Slope\_y)'_z\kappa$, (c) $(Slope\_y)_z\kappa'$ and (d) $(Slope\_y)'\kappa'_z$. The right column is the same as the left column, but for the EG experiment. (Unit: 10^{-2} cm s^{-1})

Figure 9 The zonal-averaged meridional density slope for (a) K500, (b) K1000, (c) FMH3D, (d) FMH4D, and (e) EG during 1960–1969. The difference in the zonal-averaged meridional density slopes between 1960–1969 and 1998–2007 for (f) K500, (g) K1000, (h) FMH3D, (i) FMH4D, and (j) EG. The zonal-averaged vertical variation of the meridional density slope for (k) K500, (l) K1000, (m) FMH3D, (n) FMH4D, and (o) EG. The difference in the zonal-averaged vertical variation of the meridional density slope between 1960–1969 and 1998–2007 for (p) K500, (q) K1000, (r) FMH3D, (s) FMH4D, and (t) EG.

Figure S1. (a) The black line is the 12-month running mean zonal wind stress averaged in the Southern Ocean (40°S–60°S and 0–360°E) from LICOML. The thick black line is the linear trend of the monthly series. The red line and the thick red line are same as the black line and the thick black line but for LICOMH.

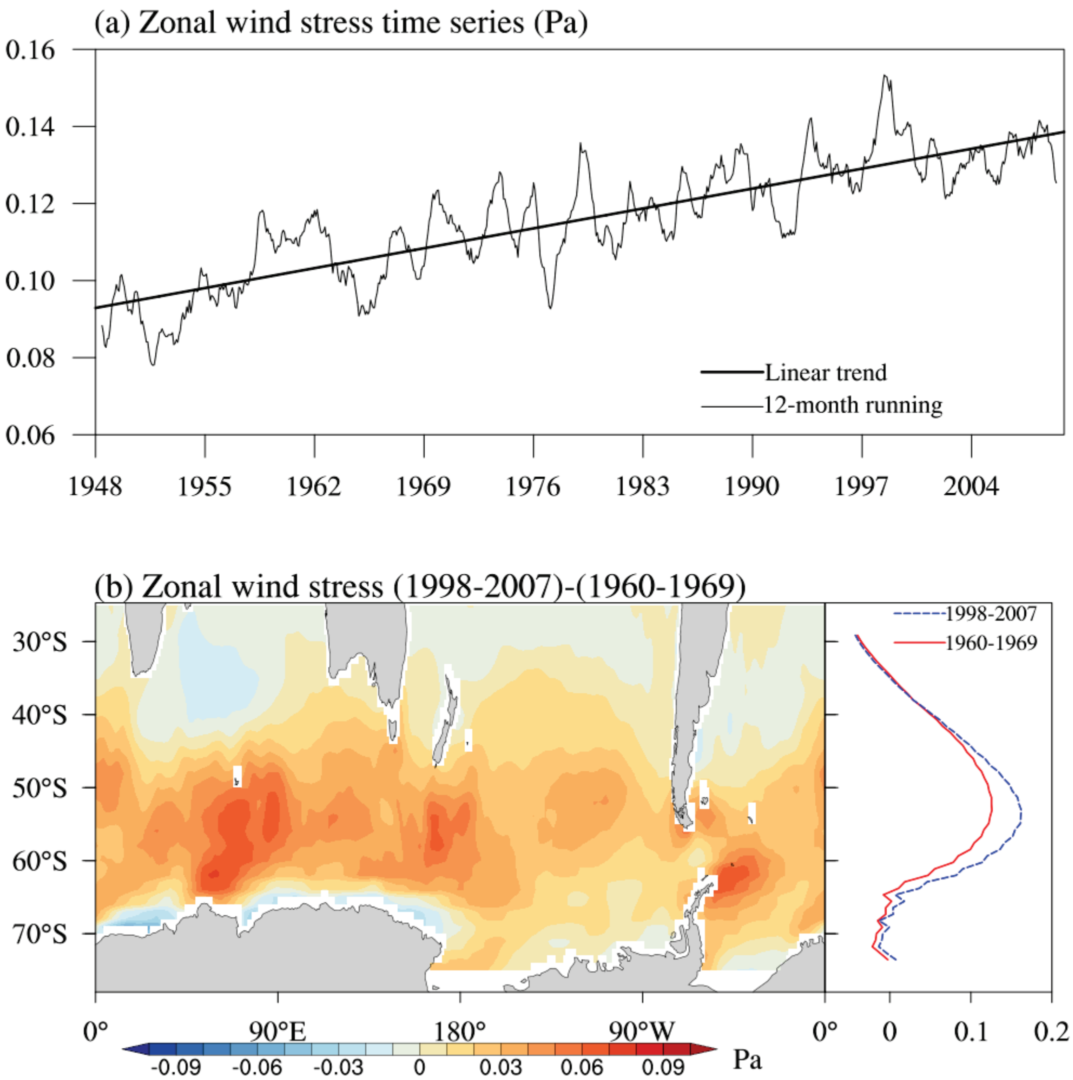

806 **Figure 1**

807

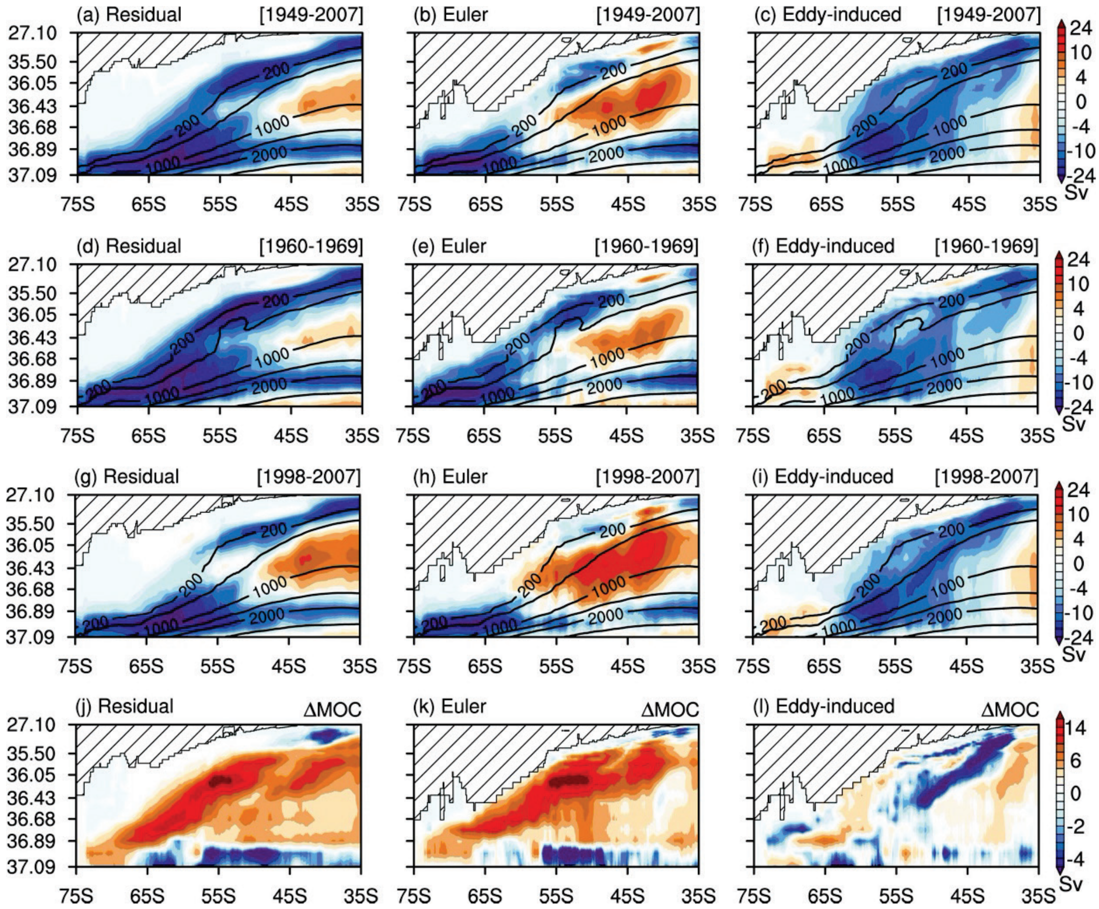
(a) Residual
[1949-2007]
(b) Euler
[1949-2007]
(c) Eddy-induced
[1949-2007]
(d) Residual
[1960-1969]
(e) Euler
[1960-1969]
(f) Eddy-induced
[1960-1969]
(g) Residual
[1998-2007]
(h) Euler
[1998-2007]
(i) Eddy-induced
[1998-2007]
(j) Residual
ΔMOC
(k) Euler
ΔMOC
(l) Eddy-induced
ΔMOC
27.10
35.50
36.05
36.43
36.68
36.89
37.09
75S
65S
55S
45S
35S
200
1000
2000
24
10
4
0
-4
-10
-24
14
6
0
-2
-4
Sv

Figure 2

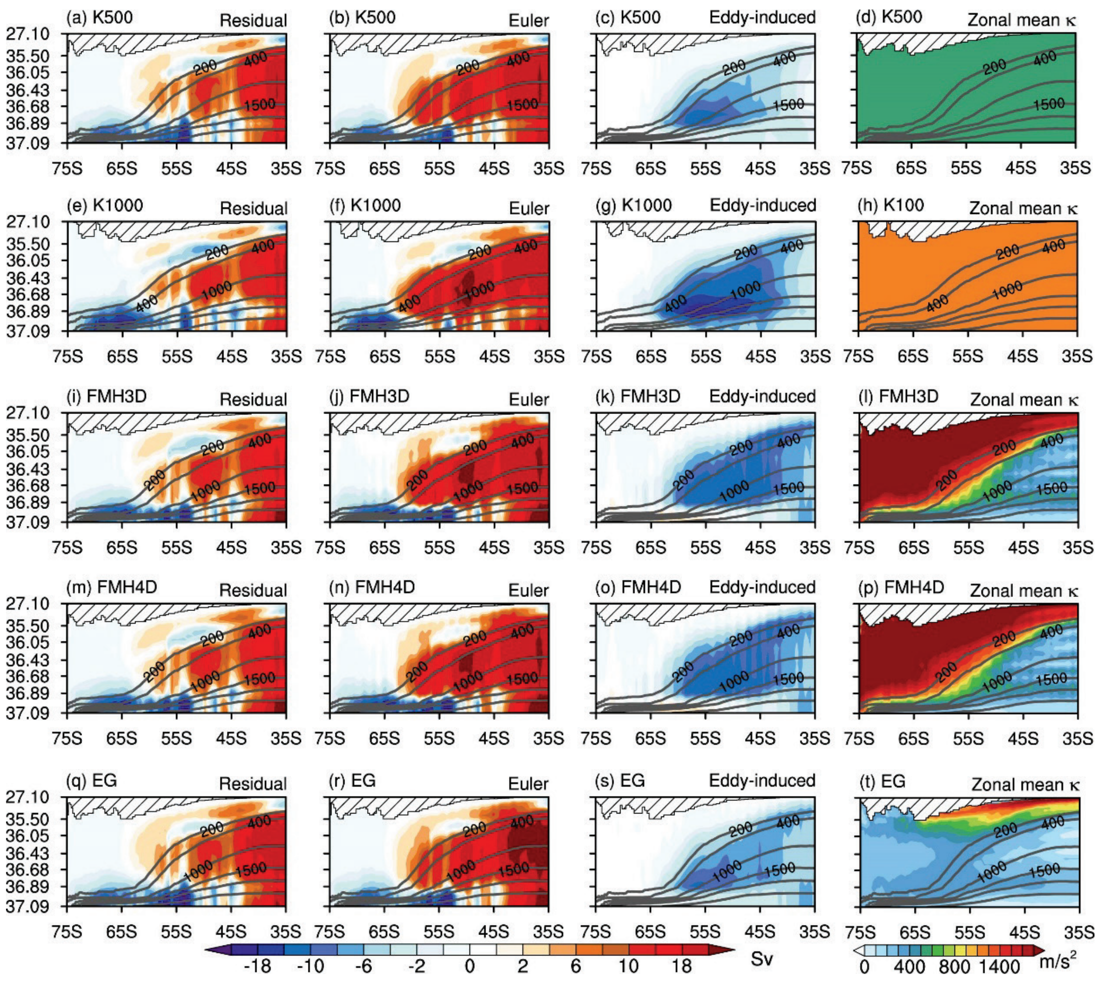
(a) K500
Residual
(b) K500
Euler
(c) K500
Eddy-induced
(d) K500
Zonal mean κ
(e) K1000
Residual
(f) K1000
Euler
(g) K1000
Eddy-induced
(h) K100
Zonal mean κ
(i) FMH3D
Residual
(j) FMH3D
Euler
(k) FMH3D
Eddy-induced
(l) FMH3D
Zonal mean κ
(m) FMH4D
Residual
(n) FMH4D
Euler
(o) FMH4D
Eddy-induced
(p) FMH4D
Zonal mean κ
(q) EG
Residual
(r) EG
Euler
(s) EG
Eddy-induced
(t) EG
Zonal mean κ
27.10
35.50
36.05
36.43
36.68
36.89
37.09
75S 65S 55S 45S 35S
200
400
1000
1500
-18 -10 -6 -2 0 2 6 10 18
Sv
0 400 800 1400
m/s2

Figure 3

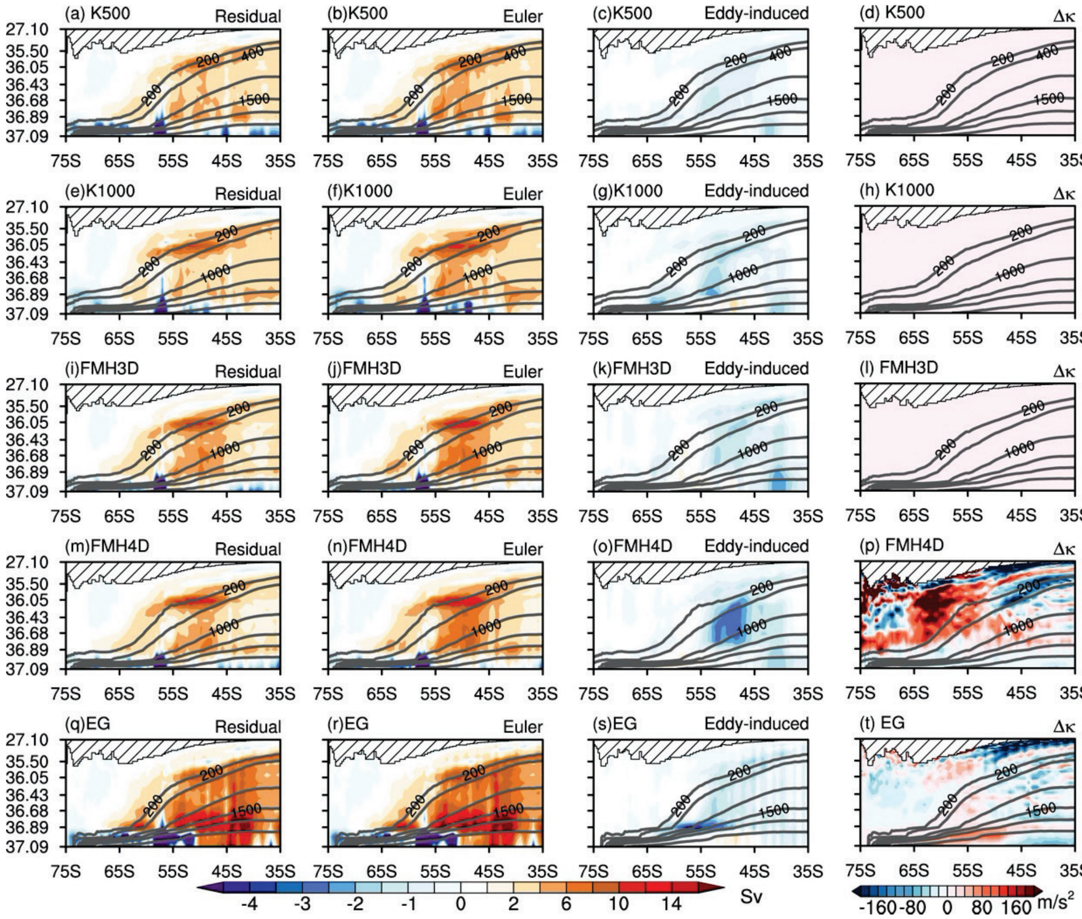

815 **Figure 4**

816

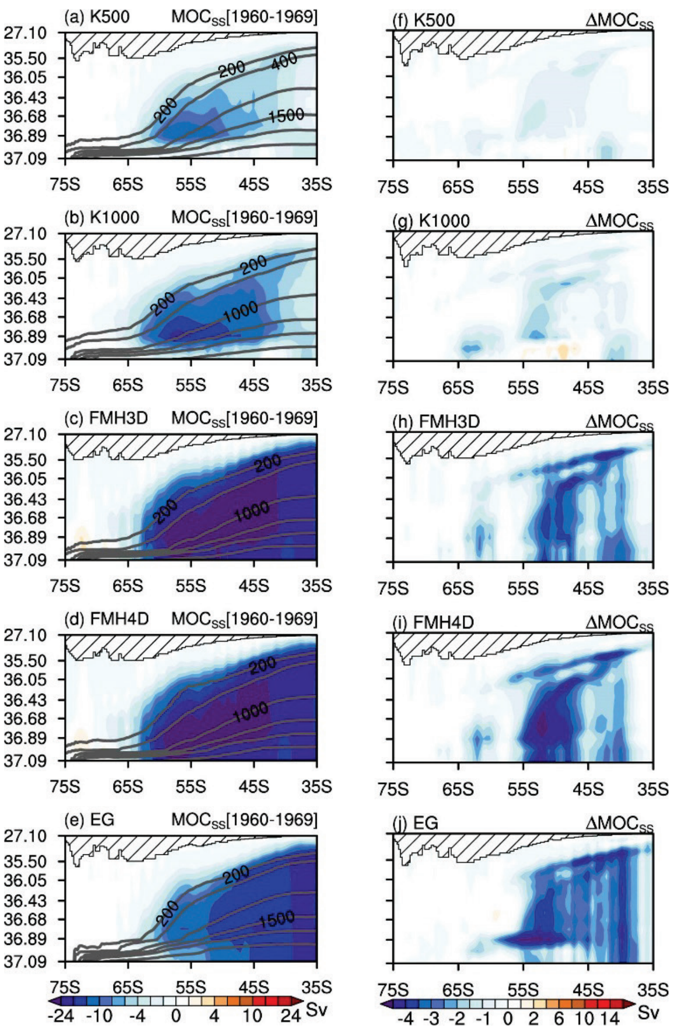

818 **Figure 5**

819

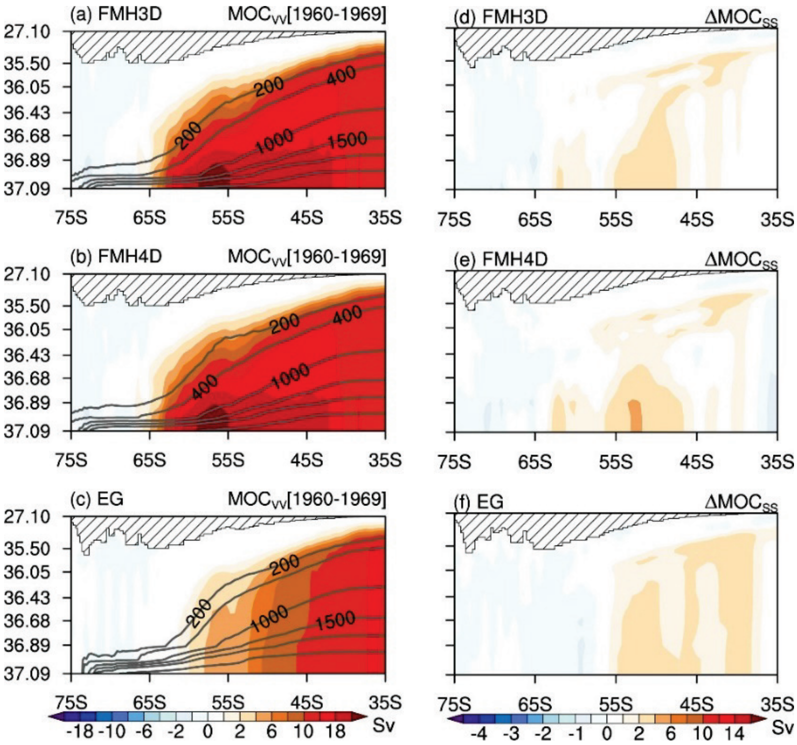

821 **Figure 6**

822

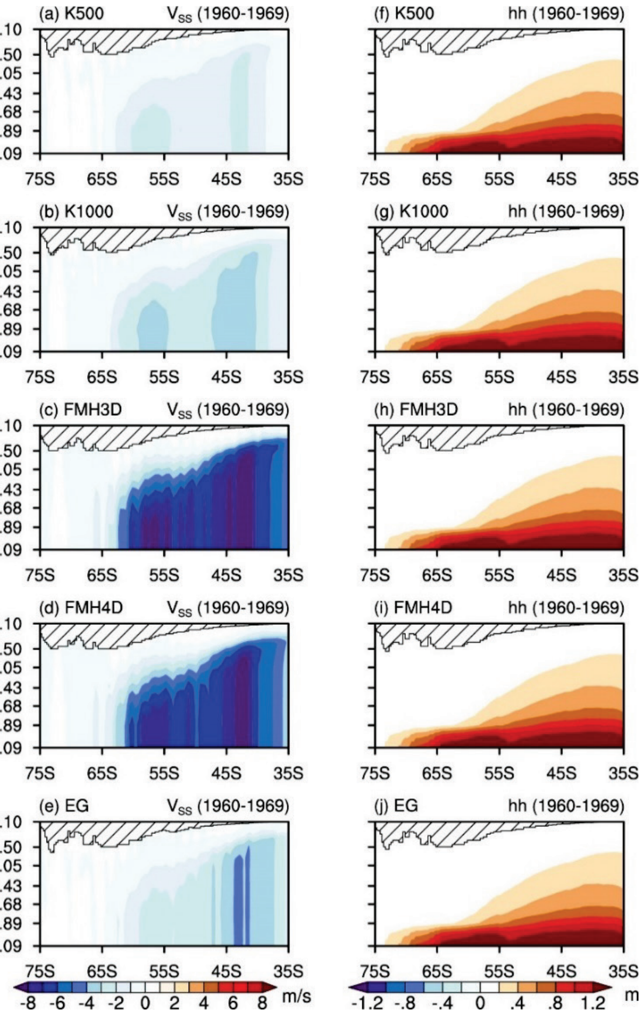

(a) K500
V_{SS} (1960-1969)
(b) K1000
V_{SS} (1960-1969)
(c) FMH3D
V_{SS} (1960-1969)
(d) FMH4D
V_{SS} (1960-1969)
(e) EG
V_{SS} (1960-1969)
(f) K500
hh (1960-1969)
(g) K1000
hh (1960-1969)
(h) FMH3D
hh (1960-1969)
(i) FMH4D
hh (1960-1969)
(j) EG
hh (1960-1969)
27.10
35.50
36.05
36.43
36.68
36.89
37.09
75S 65S 55S 45S 35S
-8 -6 -4 -2 0 2 4 6 8 m/s
-1.2 -.8 -.4 0 .4 .8 1.2 m

Figure 7

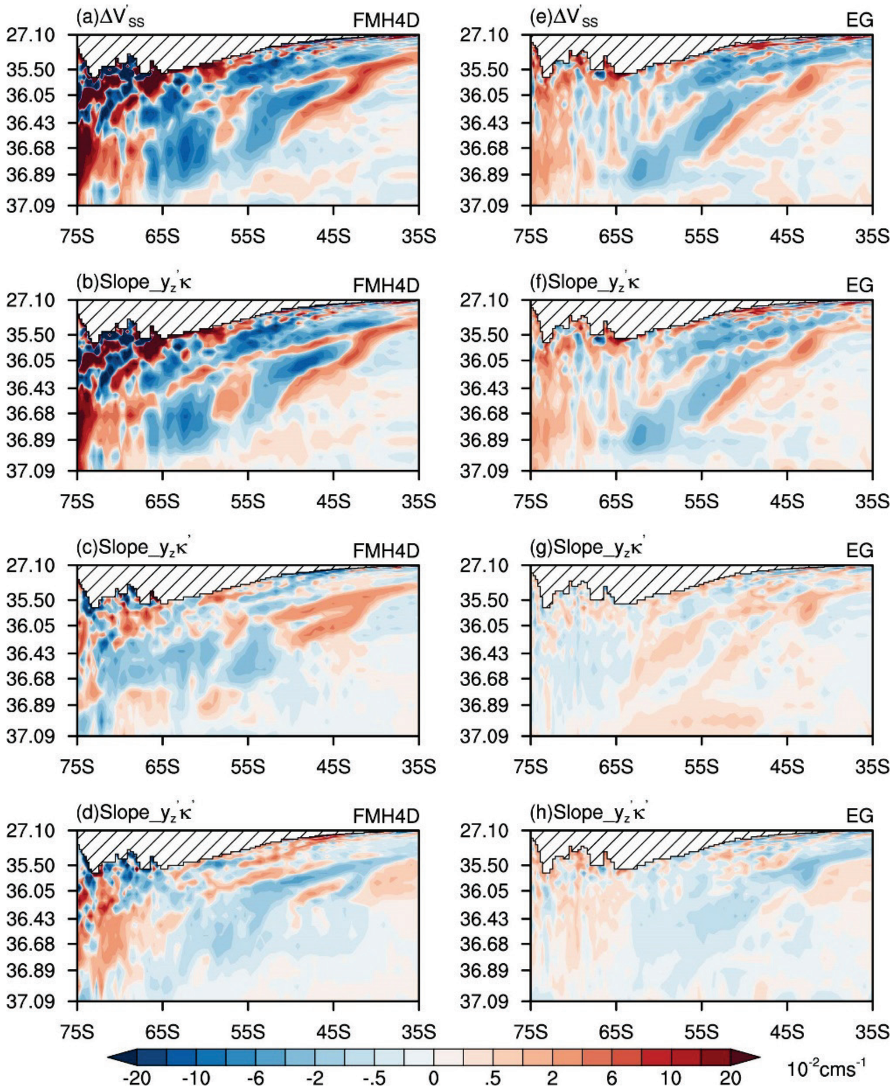
(a)ΔV'ss
FMH4D
(e)ΔV'ss
EG
(b)Slope_y'zκ
FMH4D
(f)Slope_y'zκ
EG
(c)Slope_yzκ'
FMH4D
(g)Slope_yzκ'
EG
(d)Slope_y'zκ'
FMH4D
(h)Slope_y'zκ'
EG
27.10
35.50
36.05
36.43
36.68
36.89
37.09
75S
65S
55S
45S
35S
-20
-10
-6
-2
-.5
0
.5
2
6
10
20
10^-2cms^-1

Figure 8

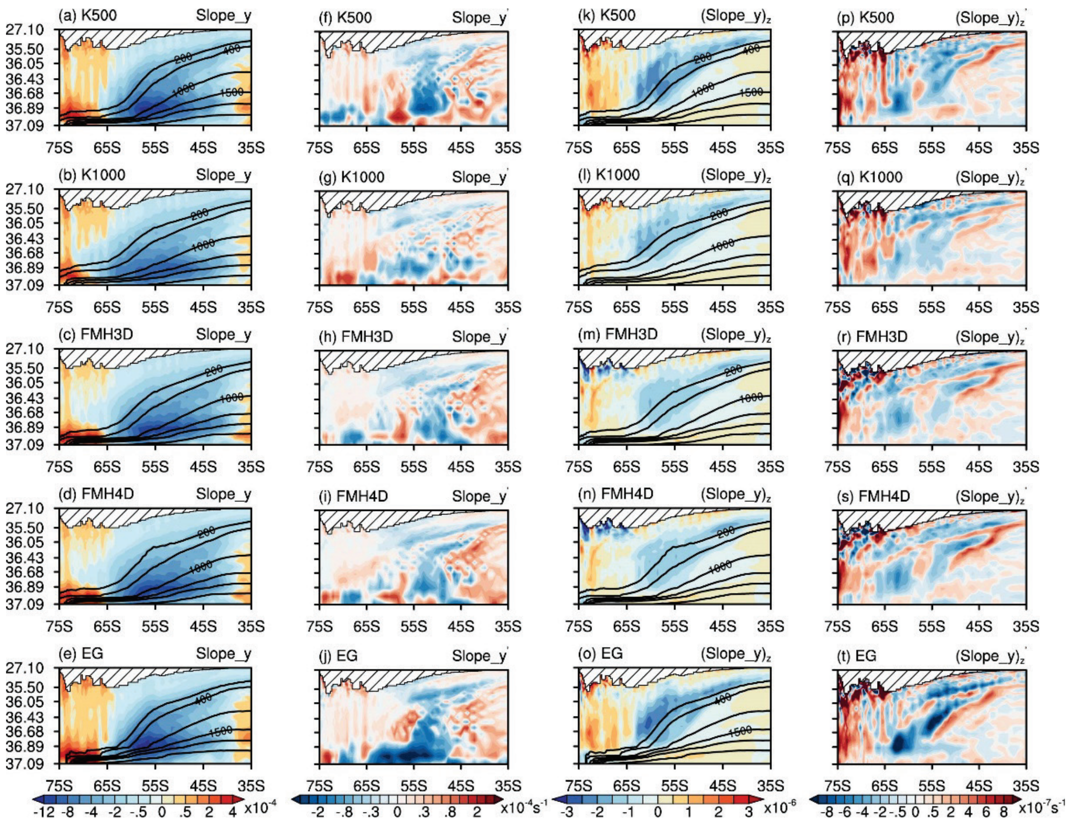

(a) K500 Slope_y
(b) K1000 Slope_y
(c) FMH3D Slope_y
(d) FMH4D Slope_y
(e) EG Slope_y
(f) K500 Slope_y'
(g) K1000 Slope_y'
(h) FMH3D Slope_y'
(i) FMH4D Slope_y'
(j) EG Slope_y'
(k) K500 (Slope_y)z
(l) K1000 (Slope_y)z
(m) FMH3D (Slope_y)z
(n) FMH4D (Slope_y)z
(o) EG (Slope_y)z
(p) K500 (Slope_y)z'
(q) K1000 (Slope_y)z'
(r) FMH3D (Slope_y)z'
(s) FMH4D (Slope_y)z'
(t) EG (Slope_y)z'
27.10 35.50 36.05 36.43 36.68 36.89 37.09
75S 65S 55S 45S 35S
-12 -8 -4 -2 -.5 0 .5 2 4 x10-4
-2 -.8 -.3 0 .3 .8 2 x10-4s-1
-3 -2 -1 0 1 2 3 x10-6
-8 -6 -4 -2 -.5 0 .5 2 4 6 8 x10-7s-1

Figure 9

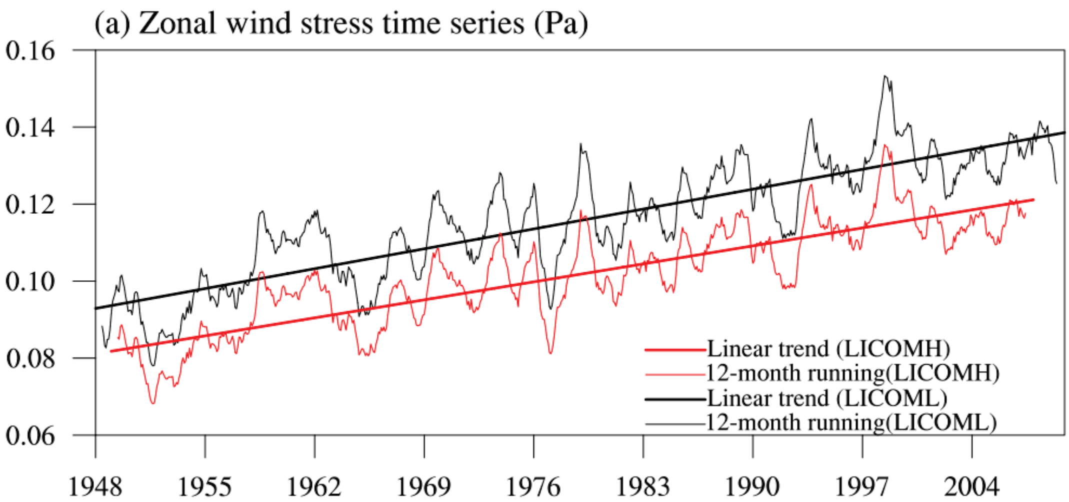
(a) Zonal wind stress time series (Pa)
0.16
0.14
0.12
0.10
0.08
0.06
1948
1955
1962
1969
1976
1983
1990
1997
2004
Linear trend (LICOMH)
12-month running(LICOMH)
Linear trend (LICOML)
12-month running(LICOML)

Figure S1.